Journal of Alloys and Compounds 664 (2016) 45–58

Contents lists available at ScienceDirect

Journal of Alloys and Compounds

journal homepage: http://www.elsevier.com/locate/jalcom

Effects of TiO_2 powder morphology on the mechanical response of pure magnesium: 1D nanofibers versus 0D nanoparticulates

Ganesh Kumar Meenashisundaram [a], Mui Hoon Nai [a], Abdulhakim Almajid [b], Khalil Abdelrazek Khalil [b], Hany S. Abdo [b], Manoj Gupta [a, *]

[a] Department of Mechanical Engineering, National University of Singapore, 9 Engineering Drive 1, Singapore 117576, Singapore
[b] Mechanical Engineering Department, College of Engineering, King Saud University, P O Box 800, Riyadh 11421, Saudi Arabia

ARTICLE INFO

Article history:
Received 8 July 2015
Accepted 22 December 2015
Available online 24 December 2015

Keywords:
Magnesium nanocomposites
TiO_2 morphology
Nanoparticulates
Nanofibers
Tensile loading
Compression loading

ABSTRACT

A novel attempt is made to study and compare the effects of TiO_2 morphology in the form of nanoparticulates and nanofibers on the physical, mechanical and microstructural properties of pure magnesium. Pure magnesium and Mg (1.98 and 2.5) vol. % TiO_2 nanocomposites are synthesized by powder metallurgy technique coupled with microwave sintering followed by hot extrusion. X-Ray diffraction studies of the synthesized magnesium materials indicated that morphology of ultrafine reinforcements play a vital role in modifying the strong basal texture of pure magnesium. The microstructural characterization of Mg–TiO_2 nanocomposites indicated significant grain refinement of pure Mg with TiO_2 nanoparticulates contributing more effectively exhibiting as high as 22% reduction observed with Mg 2.5 vol. % TiO_2 nanocomposite having TiO_2 in the form of nanoparticulates. Under tensile loading, with addition of 1.98 vol. % TiO_2 nanoparticulates and nanofibers, significant improvement in the tensile fracture stain of pure magnesium of ~14.5% and ~13.5%, respectively was observed. Further, marginal changes in the tensile strength of pure magnesium by ~10 MPa was observed with the addition of TiO_2 reinforcements. Under compression loading, among the synthesized magnesium materials, Mg–TiO_2 nanocomposites containing 1.98 vol. % TiO_2 nanofibers exhibited superior strength properties with a maximum 0.2% compressive yield strength and ultimate compressive strength of ~90 MPa and ~300 MPa, respectively. Further, decrease in the tension-compression asymmetry values was found to be more significant in Mg–TiO_2 nanocomposites where TiO_2 was used in the fiber form. The results reveal that TiO_2 nanofiber is more effective in improving the overall mechanical performance of pure magnesium.

1. Introduction

Metals and alloys play a huge role due to their wide spread applications in the areas of science and technology including electronics, energy, sports, health care and aviation. It is of prime importance to synthesize and investigate on new materials especially targeting towards weight critical applications to reduce fuel consumption and thereby mitigating greenhouse gas emissions. Magnesium is the lightest of all the available structural metals having a density of 1.74 g/cm^3. It is the sixth most abundant element in the earth's crust contributing approximately to 2.7% by weight. Several other benefits of magnesium include excellent castability, machinability, high damping capacity, thermal stability and resistance to electromagnetic radiation. Low density and high specific mechanical properties of magnesium materials make them potential candidates for structural applications. Further, magnesium materials exhibits low elastic modulus (~45 GPa) closer to that of natural bone, ability to degrade in vivo without toxicity and excellent biocompatibility, thereby making them more suitable implant materials especially targeting towards orthopedic applications [1]. However, at room temperature, limited ductility of magnesium materials poses a major threat to its extensive applications in engineering sectors.

The deformation behavior of magnesium materials having hexagonal crystal structure (HCP) is strongly affected by the presence of possible deformation mechanisms such as basal slip, prismatic slip, pyramidal slip and several twinning modes [2]. In addition to slip, plastic deformation in magnesium materials is often accommodated by twinning [3]. The directional nature of

* Corresponding author.
E-mail address: mpegm@nus.edu.sg (M. Gupta).

http://dx.doi.org/10.1016/j.jallcom.2015.12.176
0925-8388/

twinning makes magnesium materials to get deformed exhibiting large anisotropy under different initial stress states and textures [4,5]. The level of anisotropy can be captured by measuring the tensile-compression anisotropy (TCA) value which is $\sigma_{y,t}/\sigma_{y,c}$, where $\sigma_{y,t}$ and $\sigma_{y,c}$ are uniaxial tensile and compressive yield strengths respectively [3]. Over the period of years, tremendous efforts towards improving the mechanical properties of magnesium materials have been made by employing effective synthesis methodologies, through grain refinement, alloying and addition of secondary particulates and among which, composite approach utilizing ultrafine dispersed powder particulates is considered as a promising technique [6]. Dispersion strengthening or strengthening from fine particulates is proven to be an effective method for improving the mechanical response of magnesium materials for which selection of suitable particulate reinforcements is of prime importance [7].

Two main characteristics of powder on which its properties and their potential areas of applications depend are: (a) powder size or particle size (granulometry) and (b) particle shape (morphology). Particle size can be of the range: (a) micron (1×10^{-6} to 100×10^{-6} m), (b) sub-micron (0.1×10^{-6} to 1×10^{-6} m) and (c) nano (1×10^{-9} to 100×10^{-9} m). Due to the alluring advantages of particle size, researchers were able to fine tune the base material property to their interest through composite approach. Over a period of years, many works on studying the effect of particle size of both metallic and ceramic reinforcement powders on the mechanical response of magnesium materials have been investigated [8–13]. Particle shape of the powder can be: (a) regularly shaped such as spherical or (b) irregularly shaped such as ellipsoid, angular, dendritic etc. The recent advancements in the areas of microscopy enable researchers to understand nanoscale materials more effectively. Special attention was on synthesis and characterization of materials containing particulates of nano-length scale due to their larger surface area with possibilities of higher surface contact with the metal matrix. Based on the number of dimensions, the nanomaterials can be classified as: (a) zero-dimensional (0-D) or dimensionless such as nanoparticles (NPs), (b) one-dimensional (1-D) with needle-like shaped such as nanofibers (NFs), nano tubes, nano wires and nano rods, (c) two-dimensional (2-D) with plate-like shaped such as nano films and (d) three-dimensional (3-D) or bulk nanomaterials.

Nanofibers are one of the advanced and very promising nanomaterials with high specific area owing to their small diameters and are used for wide range of applications including biomedicine especially in tissue engineering, wound healing and drug delivery [14]. Several methods have been developed for fabrication of nanofibers such as [15]: (a) template [16], (b) self-assembly [17], (c) phase separation [18], (d) melt-blowing [19] and (e) electro spinning [20–22]. Among the fabrication methodologies, electrospinning is considered as the most promising technique for synthesizing large scale continuous fibers with fiber diameter in the range of few nanometers to micrometers [15]. It is a simple and most versatile method for producing rich variety of ultrathin fibers including polymers, ceramics and composites [23]. Further, unlike dispersion strengthened materials, fiber-strengthened materials contain high modulus fibers that can carry the entire load transmitted by the matrix [24]. Titania (TiO_2) exhibits high mechanical resistance, biocompatibility, chemical inertness, chemical stability in aqueous environments and available at low cost [25–28]. It is a bioactive material and a preferred reinforcement for improving the bioactivity of composites targeting biomedical applications exhibiting low toxicity to aquatic organisms [1,29]. The results of the literature search, however, reveal that no attempt is made so far to study and compare the isolated effects of titania nanofibers (1-D) and titania nanoparticulates (0-D) on altering the CTE, hardness, tensile and compressive response of monolithic pure magnesium synthesized by powder metallurgy technique in the absence of microstructural factors related to the presence of precipitates and heat treatment.

Accordingly, in the present study, Mg nanocomposites containing (1.98 and 2.5) vol. % TiO_2 reinforcements in the form of NFs and NPs are synthesized by utilizing powder metallurgy technique coupled with microwave sintering process followed by hot extrusion. The physical, microstructural and mechanical properties of the nanocomposites are studied and compared. The level of anisotropy/asymmetry in the synthesized pure Mg and Mg–TiO_2 nanocomposites containing NFs and NPs is observed through measurement of TCA values.

2. Materials and methods

2.1. Materials

In the present study, for the base material, magnesium (Mg) powder of purity > 98.5% with a size range of 60–300 μm supplied by Merck, Germany was utilized. For reinforcement phase, required amount of pure titanium dioxide (TiO_2) nanopowder of size ~ 21 nm and purity > 99.5% supplied by Sinopharm Chemical Reagent Co., Ltd, China and TiO_2 nanofibers synthesized by electrospinning process (as discussed under *Section 2.2*) with an average length and diameter of ~1.5 μm and ~80 nm, respectively were utilized.

2.2. Synthesis of TiO_2 nanofibers

Fabrication of TiO_2 nanofibers involves three steps: (a) preparation of sol–gel, (b) electrospinning at 20 KV, 50 rpm, and (c) calcination process.

2.2.1. Preparation of sol–gel

Initially, mixture of 4.5 g of titanium (IV) isopropoxide (C_{12} H_{28} O_4 Ti) and ratio of 9 g acetic acid to 30 g ethanol containing 1.5 g of polyvinylpyrrolidone (PVP) was vigorously stirred at room temperature for 2 h to obtain 45 g of homogeneous polymer solution. A transparent solution (gelatin) was then prepared by stirring N,N-dimethylformamide (DMF) containing 7 wt. % polyacrylonitrile (PAN) for 2 h. Finally, Sol–gel is obtained by vigorous stirring of the initial mixture with gelatin at room temperature for 2 h and is then introduced into the electrospinning machine.

2.2.2. Electrospinning

A typical electrospinning setup consisting of a mechanical needle with a small orifice (~1 mm) connected to the sol–gel reservoir, high voltage supplier (20 KV) and an electrically ground rotating drum or collector (50 rpm) was utilized in this study (Fig. 1). Mechanical needle (syringe) is used to inject the sol–gel directed towards the rotating drum. The orifice of the needle is connected to a high voltage (20 KV) for obtaining electrically charged jet of polymer solution. The solution jet solidifies or evaporates before reaching the collecting drum. Stretching of the viscoelastic thread under the electric field combined with solvent evaporation leads to the formation of TiO_2/PVP nanofibers and is deposited on the grounded collector. The morphology of as-spun nanofibers was studied by using a scanning electron microscope (SEM) (Fig. 2) indicating regular morphology with smooth surface having an average diameter of ~80 nm. Further, the energy dispersive X-ray spectroscopy (EDS) analysis identifies titanium (Ti) as an elemental component in the fibers indicating: (a) Ti ions embedded in the PVP polymer matrix and (b) Ti is loaded without any chemical or structural modifications into PVP polymer matrix

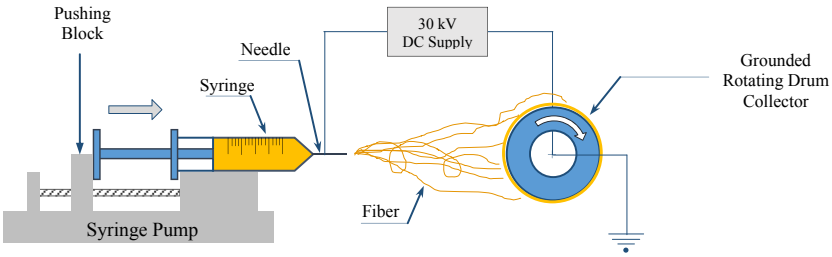

Fig. 1. Schematic diagram of electrospinning process.

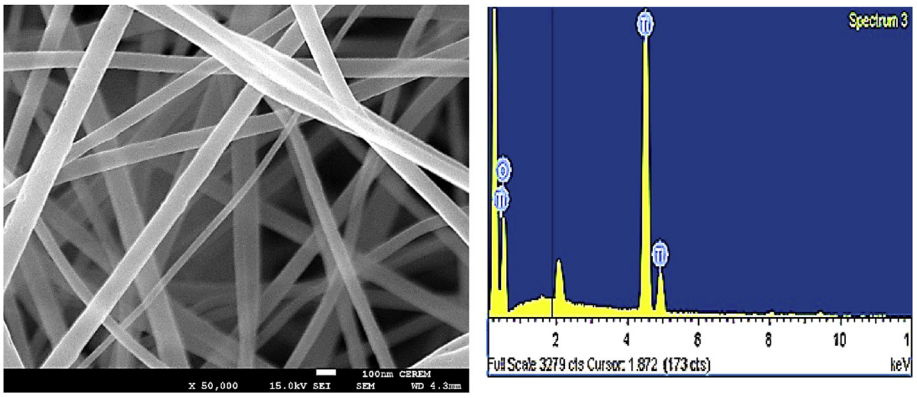

Fig. 2. SEM and EDS images of as-spun PVP/TTIP nanofibers before calcination.

to form an organic – inorganic nanocomposite.

2.2.3. Calcination

Calcination process was performed by using tube furnace (CARBOLITE Type 3216CC). The as-spun fibers obtained were initially dried for 12 h at 75 °C under vacuum. In order to remove the polymer binder used in synthesizing sol–gels, the samples were calcined in air atmosphere at 600 °C for 3 h utilizing heating rate of 10 °C/min. Further, the average fiber dimension and aspect ratio were determined by tapping mode imaging using a Dimension 3100 Atomic Force Microscope (AFM) (Bruker, USA) on more than 15 fibers. The nanofibers were initially dispersed in ethanol by sonification and later drop cast on a mica substrate and dried in a vacuum dessicator prior to measurements. When compared to that of TiO_2 nanofibers obtained by as-spun condition (Fig. 2), nil or minimal changes in the dimensions of nanofibers (Fig. 3) was observed and is further confirmed from the representative AFM image (Fig. 4).

Fig. 4 shows the granulometry of TiO_2 nanoparticulate and nanofiber measured by utilizing Atomic Force Microscopy. The shape and size of TiO_2 nanoparticulate was found to be ellipsoidal with average diameter of ~21 nm.

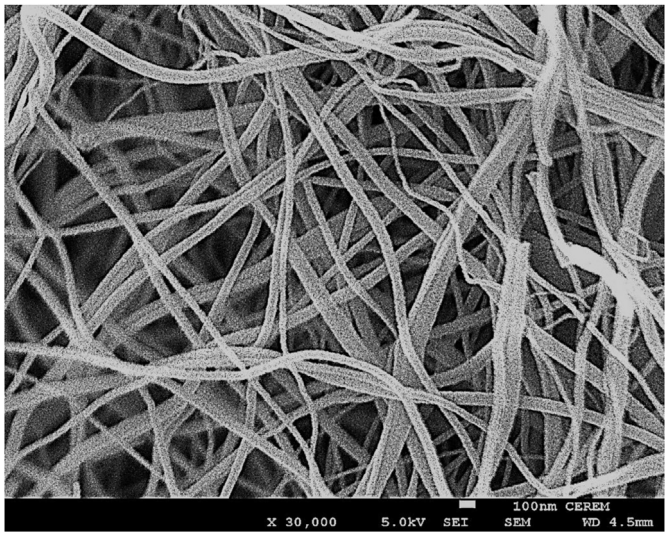

Fig. 3. SEM images for TiO_2 nanofiber after calcination at 600 °C.

2.3. Processing of Mg–TiO_2 nanocomposites

2.3.1. Primary processing

In the present study, Mg (1.98 and 2.5) vol. % TiO_2 nanocomposites containing TiO_2 in the form of NPs and NFs were primarily synthesized utilizing blend-press-sinter powder metallurgy technique. For synthesizing nanocomposites, initially, pure magnesium powder was blended with an appropriate amount of TiO_2 NPs and NFs in a RETSCH PM-400 mechanical alloying machine at 200 rpm for 1 h. The homogenized powder mixtures of Mg and reinforcements were then cold compacted at a pressure of ~1000 MPa to form billets of 40 mm in height and 35 mm in diameter. Monolithic magnesium was compacted using the same parameters without blending. Finally, the compacted billets were sintered using hybrid microwave sintering technique [1]. The billets were then heated to 640 °C in a 900 W, 2.45 GHz SHARP microwave oven.

2.3.2. Secondary processing

Before extrusion, the machined ingots and the sintered billets were soaked at 400 °C for 1 h in a constant temperature furnace. Using a 150 T hydraulic press, hot extrusion was carried out at 350 °C die temperature, with an extrusion ratio of 20.25:1 for

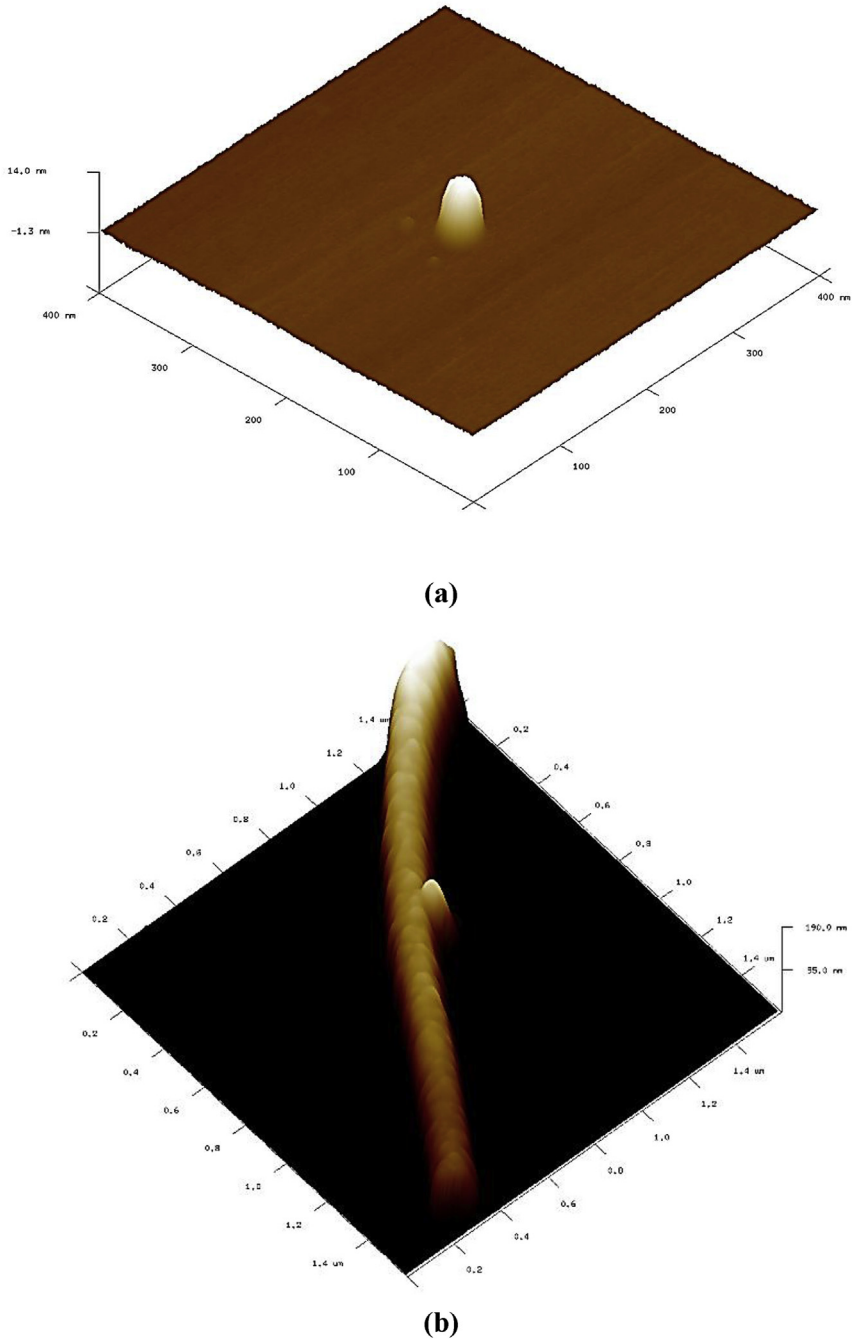

Fig. 4. Granulometry of TiO_2 (a) nanoparticulate and (b) nanofiber measured using Atomic Force Microscopy.

obtaining rods of 8 mm in diameter. The samples from the extruded rods were used for characterization, as detailed in the next section.

2.4. Materials characterization

2.4.1. Density measurements

Density of extruded pure Mg and Mg–TiO_2 nanocomposites in polished condition was measured using Archimedes principle. Three samples from different ends of the extruded rods were accurately weighed in air and then immersed in distilled water. An A&D ER-182A electronic balance with an accuracy of 0.0001 g was used for measuring the weights. Using rule of mixture principle, the theoretical densities of the synthesized Mg materials were calculated and compared with the measured experimental density values. Porosity values of the synthesized Mg materials were calculated utilizing Eq. (1).

$$Porosity = \frac{\rho_{th} - \rho_{exp}}{\rho_{th} - \rho_{air}} \times 100 \quad (1)$$

Where, ρ_{th} is the theoretical density (g/cm^3), ρ_{exp} is the experimental density in (g/cm^3) and ρ_{air} is the density of air (0.001225 g/cm^3).

2.4.2. X-Ray Diffraction studies

The extruded pure magnesium and Mg (1.98 & 2.5) vol. % TiO_2

Table 1
Density and CTE measurements of pure magnesium and synthesized Mg– TiO_2 nanocomposites.

Sl. No	Material	Reinforcement			Density measurements			CTE ($\times 10^{-6}$/K)
		Morphology	(Wt %)	(Vol %)	Theoretical density (g/cm^3)	Experimental density (g/cm^3)	Porosity (%)	
1	Mg	Nil	Nil	Nil	1.7400	1.7377	0.1322	24.72
2	Mg1.98 TiO_2	NPs	4.67	1.98	1.7892	1.7880	0.2400	24.53
		NFs	4.67	1.98		1.7845	0.2643	24.48
3	Mg 2.5 TiO_2	NPs	5.87	2.50	1.8023	1.7965	0.3220	24.42
		NFs	5.87	2.50		1.7958	0.3606	24.13

* Morphology of reinforcement such as NPs and NFs represents nanoparticulates (NPs) and nanofibers (NFs), respectively.

nanocomposite samples were exposed to Cu Kα radiation of wavelength λ = 1.54056 Å with a scan speed of 2°/min by using an automated Shimadzu lab-X XRD-6000 diffractometer. The bragg angles and the values of the interplanar spacing, d, obtained were subsequently matched with the standard values of Mg, TiO_2 and related phases. Further, the basal plane orientation of Mg–TiO_2 nanocomposites was analyzed based on the XRD peaks obtained from experiments carried out in the directions both parallel and perpendicular to the extrusion axis.

2.4.3. Microstructural characterization

To investigate on the TiO_2 reinforcement distribution within the Mg metal matrix and grain size of synthesized pure magnesium and Mg–TiO_2 nanocomposites, the microstructural characterization studies were conducted on metallographically polished extruded samples and a Hitachi S-4300 field emission scanning electron microscope (FESEM), an Olympus metallographic optical microscope and Scion image analysis software were utilized.

2.4.4. Coefficient of thermal expansion

By using a thermomechanical analysis instrument "INSEIS TMA PT 1000LT", the coefficient of thermal expansion values of pure magnesium and Mg (1.98 & 2.5) vol. % TiO_2 nanocomposites were determined. Heating rate of 5 °C/min was maintained with an argon flow rate of 0.1 lpm. By using an alumina probe, the displacement of the test samples (each of 5 mm length) was measured as a function of temperature (323 K–623 K).

2.4.5. Microhardness test

Using a Shimadzu HMV automatic digital microhardness tester with a Vickers indenter (square based pyramidal shaped diamond indenter with a phase angle of 136°), the microhardness tests were conducted on flat and metallographically polished specimens. An indenting load of 25 gf for a dwell time of 15 s was used. The testing was performed as per ASTM:E384-08.

2.4.6. Tensile test

In accordance with ASTM:E8M-01, the smooth bar tensile properties of pure magnesium and Mg (1.98 & 2.5) vol.% TiO_2 nanocomposites were determined at ambient temperature. The tensile tests were conducted on round tension test specimens of diameter 5 mm and gauge length 25 mm using a fully automated servo-hydraulic mechanical testing machine, MTS-810. The strain rate was set to 1.693×10^{-4} s^{-1} and an Instron 2630-100 series extensometer was used to measure the fracture strain. For each composition, 5 samples were tested to ensure repeatable values.

2.4.7. Compression test

In accordance with ASTM:E9-89a, the smooth bar compressive properties of the extruded pure magnesium and Mg (1.98 & 2.5) vol.% TiO_2 samples were determined at ambient temperature, using MTS-810 testing machine with a strain rate of 8.334×10^{-5} s^{-1}. The test specimens of 8 mm diameter and length to diameter ratio l/d ~1 were used. For each composition, 5 samples were tested to ensure repeatable values.

2.4.8. Fracture behavior

To provide an insight into the various possible fracture mechanisms operating during the tensile and compression loading of the samples, characterization of fractured surfaces of tensile and compression samples were successfully investigated using Hitachi S-4300 FESEM.

3. Results and discussion

3.1. Synthesis, density and porosity measurements

Fabrication of monolithic Mg and Mg–TiO_2 nanocomposites containing TiO_2 reinforcements (NPs and NFs) was successfully accomplished by utilizing powder metallurgy technique coupled with microwave sintering followed by hot extrusion. The hot extruded rods of Mg materials exhibited shiny surface with absence of circumferential defects. The observations made during the fabrication of Mg nanocomposites revealed minimal or nil oxidation which can be further confirmed through X - Ray Diffraction studies showing absence of oxides in the Mg based materials (monolithic and composites).

Density and porosity results of the synthesized pure Mg and Mg–TiO_2 nanocomposites measured from different locations of the extruded rods are shown in Table 1. From the density measurements, marginal increase in the density values of pure Mg with the addition of TiO_2 reinforcements exhibiting a maximum increase of ~3.4% with 2.5 vol. % TiO_2 addition was observed and thereby ensuring the suitability of the synthesized Mg materials for weight critical applications. A maximum porosity of ~0.36% was observed in the case of Mg 2.5 vol. % TiO_2 nanocomposites containing TiO_2 NFs. Mg nanocomposites exhibited slightly higher porosity which is due to the presence of reinforcements [30]. From the results of the density and porosity measurements, it is observed that by utilizing the adopted synthesis methodology, near dense Mg based materials can be synthesized.

3.2. X-Ray Diffraction studies

The effects of TiO_2 reinforcement morphology (NPs and NFs) on the crystallographic orientation of pure Mg is studied by utilizing X-Ray Diffraction (XRD). Fig. 5 shows the X-Ray diffractograms of the synthesized pure Mg and Mg–TiO_2 nanocomposites taken along the transverse and longitudinal sections of the hot extruded samples. The high intensity Mg peaks were prominently seen and the peaks corresponding to TiO_2 were not visible in the synthesized Mg–TiO_2 nanocomposites containing TiO_2 NPs and NFs which is due to the limitation of filtered X-ray to detect phases with low volume fraction [31]. However, the presence of TiO_2 reinforcements in Mg–TiO_2 nanocomposites can be confirmed through microstructural characterization (Figs. 6 and 7).

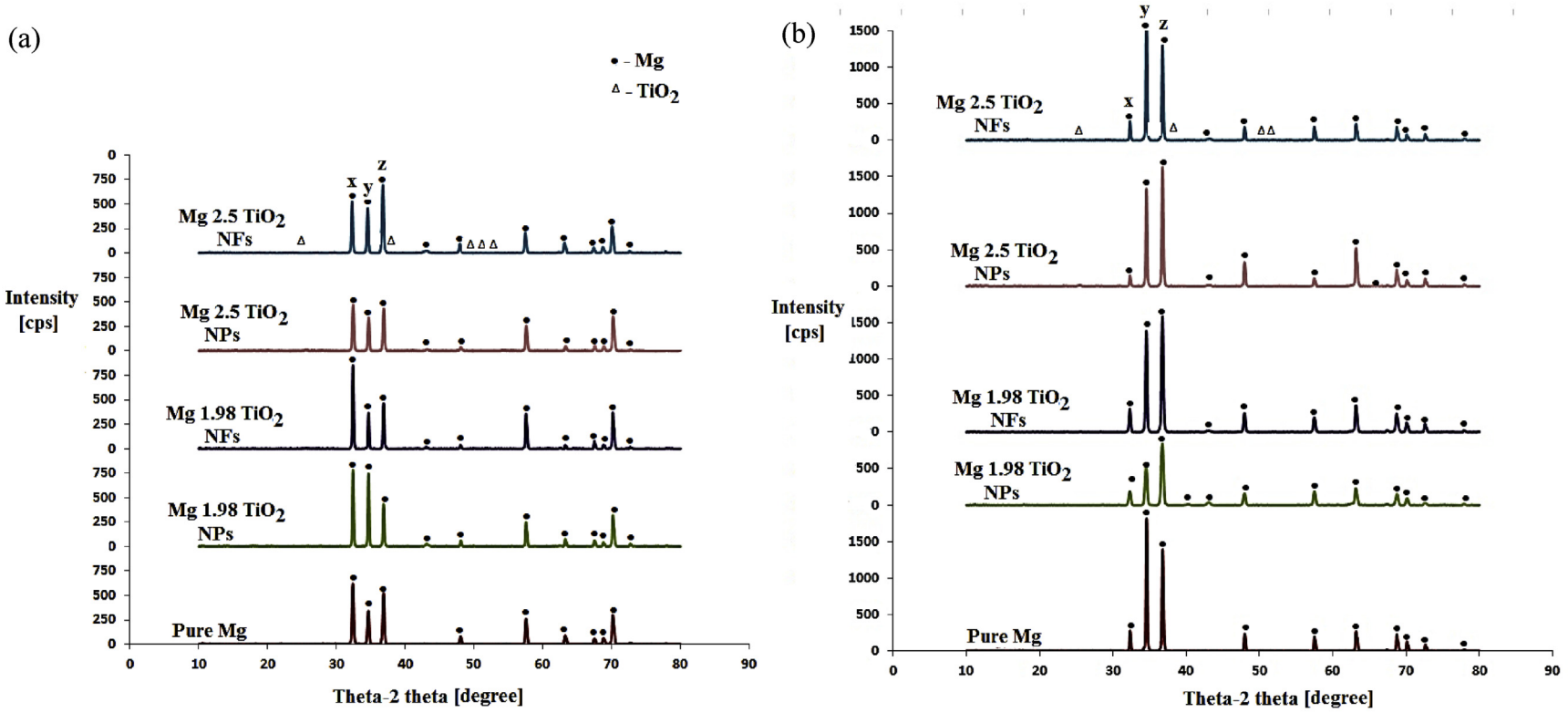

Note:

X, Y, Z represent 2θ = 32°, 34° and 36° corresponding to (1 0−1 0) prism, (0 0 0 2) basal and (1 0−1 1) pyramidal planes respectively.
Δ indicates expected intensity peaks corresponding to TiO_2 at 2θ = 25.2°, 36.9°, 48°, 53.8°, 55°.

Fig. 5. X- Ray diffractograms of pure Mg and Mg−TiO_2 nanocomposites containing NPs and NFs taken along (a) the cross sections and (b) longitudinal sections of the hot extruded samples.

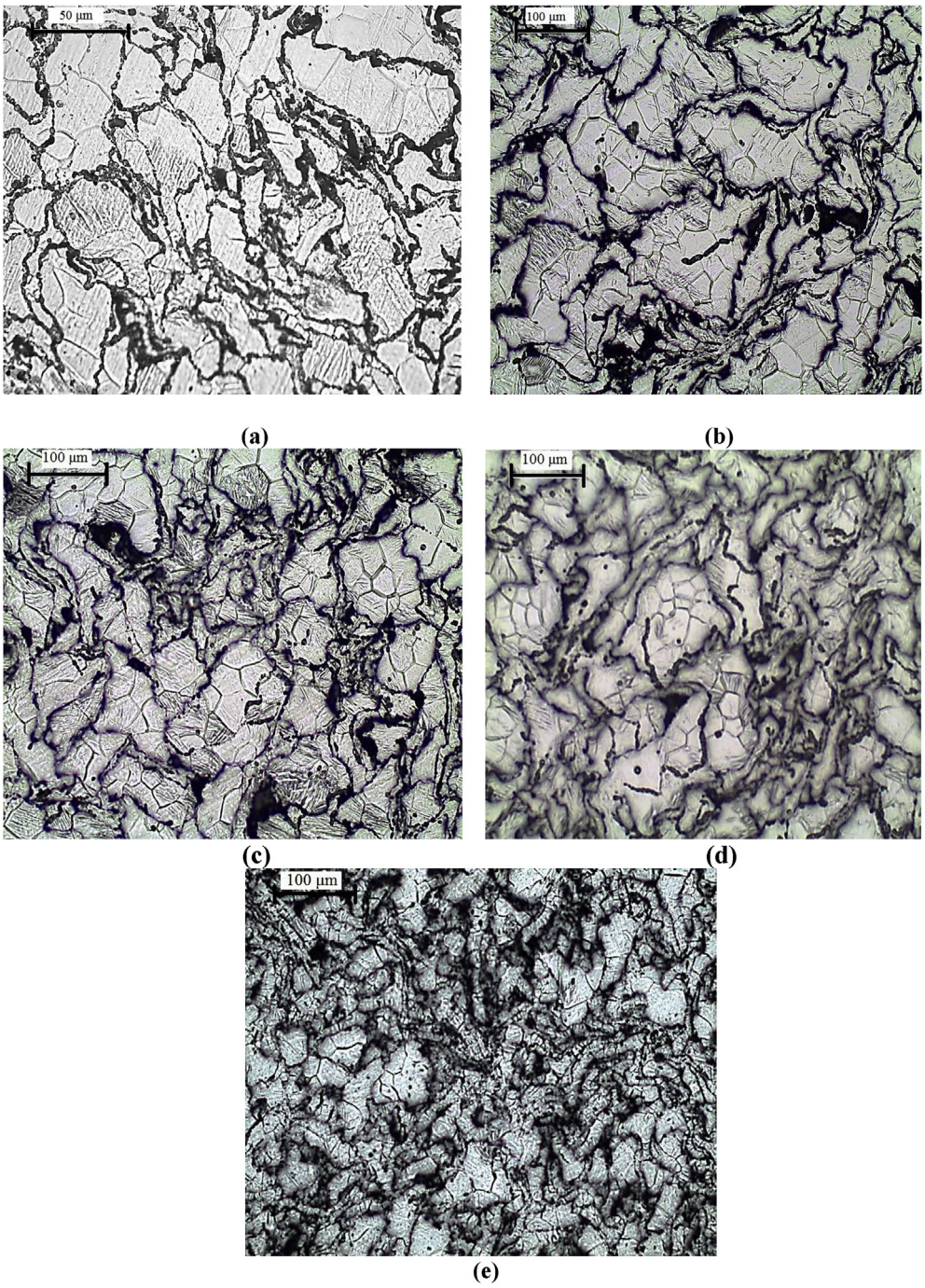

Fig. 6. Microscopic images showing grain characteristics of: (a) Pure Mg, (b) Mg1.98TiO_2 NPs (c) Mg1.98TiO_2 NFs (d) Mg2.5TiO_2 NPs (e) Mg2.5TiO_2NFs.

The ratio of maximum XRD intensity of Mg peaks to the respective prismatic (10-10), basal (0002) and pyramidal (10–11) intensities observed in the synthesized Mg materials indicated as X, Y and Z at $2\theta = 32°$, 34° and 36°, respectively (Fig. 5), taken along both the transverse and longitudinal sections of the hot extruded samples (prior to tensile and compression testing) is shown in Table 2. Along the transverse direction (perpendicular to the extrusion axis), changes in the basal plane intensity of pure Mg was observed with the addition of TiO_2 reinforcements and among the synthesized Mg–TiO_2 nanocomposites Mg 1.98 vol. % TiO_2 containing TiO_2 NPs exhibited the maximum increase in the basal plane intensity ($I_{basal}/I_{max} = 0.952$). Along the longitudinal direction (parallel to the extrusion axis), the XRD of hot extruded pure Mg exhibits strong basal texture having maximum intensity corresponding to the basal plane (at $2\theta = 34°$). The dominance of basal plane intensity in extruded pure Mg samples shows that most of the basal planes are parallel to the extrusion direction, which is commonly found in wrought Mg materials [32–34]. With the addition of TiO_2 NPs, the intensity corresponding to the pyramidal plane (at $2\theta = 36°$) increases and Mg 1.98 vol. % TiO_2 nanocomposite exhibited the lowest basal plane intensity ($I_{basal}/I_{max} = 0.655$). With further addition of TiO_2 NPs, the intensity of

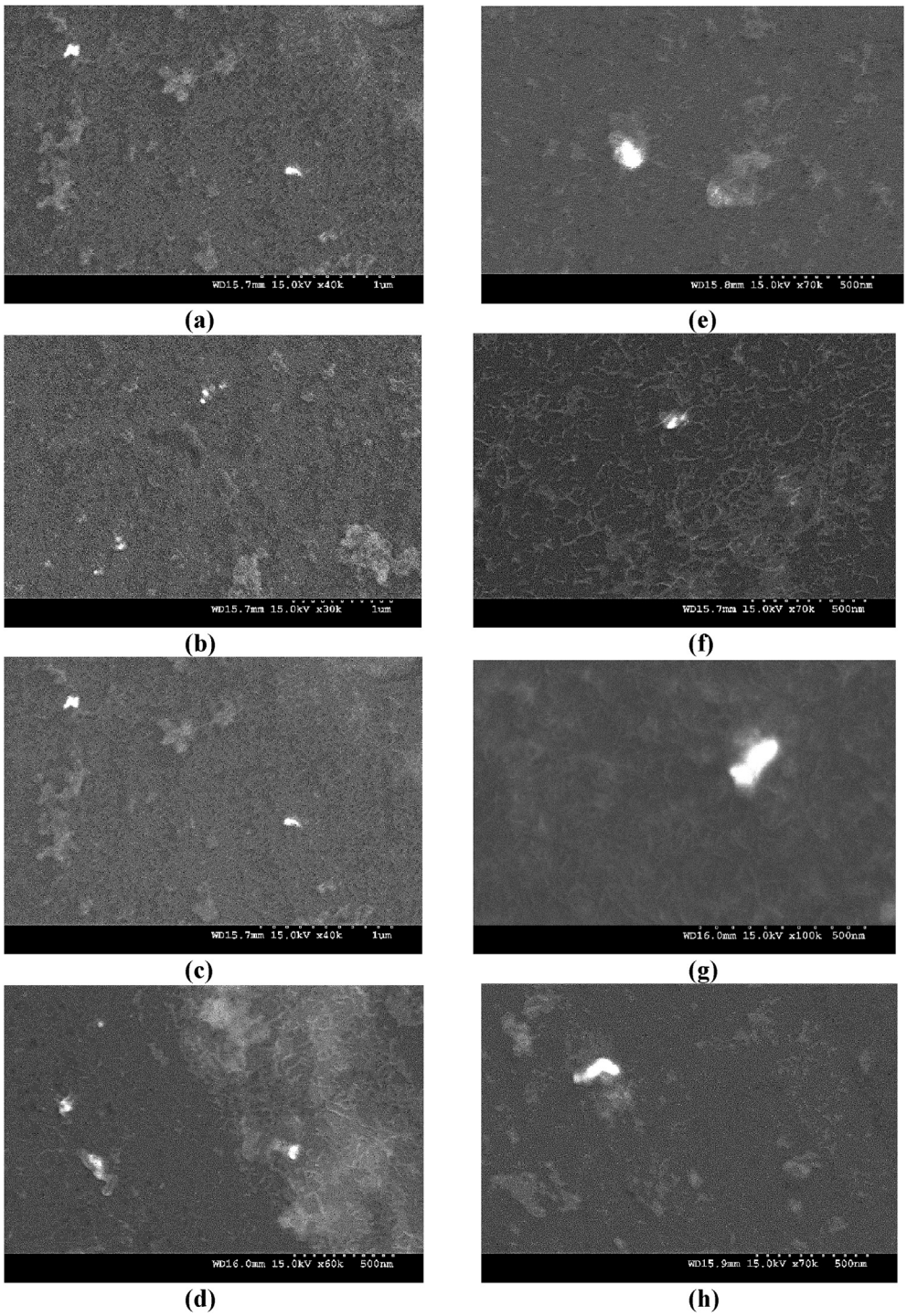

Fig. 7. Distribution of TiO_2 NPs and NFs in (a) $Mg1.98TiO_2$ NPs (b) $Mg1.98TiO_2$ NFs (c) $Mg2.5TiO_2$ NPs (d) $Mg2.5TiO_2$NFs.

basal plane increased ($I_{basal}/I_{max} = 0.844$). The dominance of pyramidal plane intensity of pure Mg observed in Mg–TiO_2 nanocomposites containing TiO_2 NPs indicate that the basal plane of pure Mg are no longer parallel to the extrusion direction. In the case of TiO_2 NFs addition, the intensity corresponding to the basal plane of pure Mg was found to decrease ($I_{basal}/I_{max} = 0.878$) with 1.98 vol. % TiO_2 and with further addition of NFs, the dominance of basal plane intensity of pure Mg was once again observed. Thus, critical amount of ultrafine reinforcements and their morphology play a vital role in modifying the basal texture of pure Mg.

3.3. Microstructure

The grain size measurements utilizing optical micrographs of etched pure Mg and Mg–TiO_2 nanocomposites containing TiO_2 reinforcements (NPs and NFs) (Fig. 6) indicate relatively finer grains in the case of Mg–TiO_2 nanocomposites when compared to that of monolithic pure Mg. With addition of TiO_2 reinforcements, the decrease in the grain size of pure Mg (Table 3) is observed which is due to: (a) the ability of TiO_2 reinforcements (NPs and NFs) to nucleate Mg grains during recrystallization and (b) presence of

Table 2
X Ray Diffractogram results of as extruded Mg–TiO_2 nanocomposites containing TiO_2 NPs and NFs.

Material	Reinforcement	Section	Plane	I/I_{max}
Pure Mg	Nil	T	10-10 Prism	1.000
			0002 Basal	0.545
			10-11 Pyramidal	0.838
		L	10-10 Prism	0.153
			0002 Basal	1.000
			10-11 Pyramidal	0.766
Mg 1.98 TiO_2	NPs	T	10-10 Prism	1.000
			0002 Basal	0.952
			10-11 Pyramidal	0.539
		L	10-10 Prism	0.214
			0002 Basal	0.655
			10-11 Pyramidal	1.000
	NFs	T	10-10 Prism	1.000
			0002 Basal	0.429
			10-11 Pyramidal	0.542
		L	10-10 Prism	0.197
			0002 Basal	0.878
			10-11 Pyramidal	1.000
Mg 2.5 TiO_2	NPs	T	10-10 Prism	1.000
			0002 Basal	0.725
			10-11 Pyramidal	0.924
		L	10-10 Prism	0.081
			0002 Basal	0.844
			10-11 Pyramidal	1.000
	NFs	T	10-10 Prism	0.755
			0002 Basal	0.656
			10-11 Pyramidal	1.000
		L	10-10 Prism	0.142
			0002 Basal	1.000
			10-11 Pyramidal	0.703

*T and L represents XRD taken along transverse and longitudinal sections of Mg–TiO_2 nanocomposites.
I_{max} is the maximum XRD intensity from either prismatic, basal and pyramidal plane.

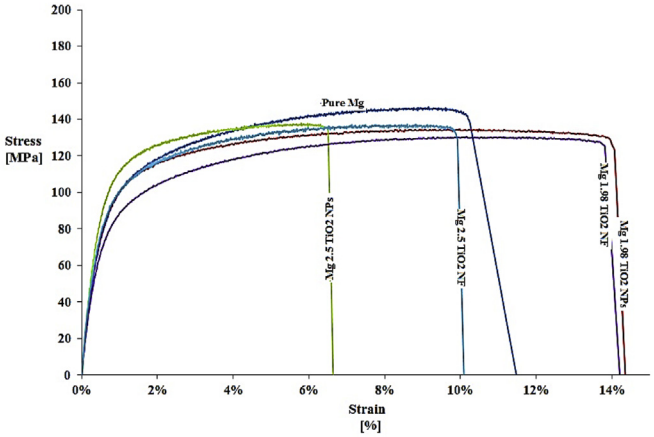

Fig. 8. Room temperature tensile properties of Mg–TiO_2 nanocomposites containing TiO_2 NPs and NFs.

case of Mg 2.5 vol. % TiO_2 NPs. Further, the distribution of TiO_2 reinforcements in the Mg–TiO_2 nanocomposites is observed through FESEM and is shown in Fig. 7 indicating minimal agglomeration of reinforcements in the composites.

3.4. Coefficient of thermal expansion (CTE)

The experimental CTE values of monolithic pure Mg and Mg (1.98 and 2.5) vol. % TiO_2 nanocomposites containing TiO_2 reinforcements (NPs and NFs) are measured in the temperature range of 50–400 °C and the results are shown in Table 1. With the addition of TiO_2 reinforcements, CTE values of pure Mg decreased

Table 3
Results of microstructure and microhardness studies.

Sl. No	Material	Grain size × 10^{-6}m	Aspect ratio × 10^{-6}m	Microhardness (Hv)
1	Mg	32 ± 1.5	1.5 ± 0.4	50 ± 2
2	Mg 1.98TiO_2 NPs	28 ± 1.5 (↓13%)	1.3 ± 0.5	60 ± 1 (↑20%)
3	Mg 1.98TiO_2 NFs	29 ± 2 (↓9%)	1.3 ± 0.5	63 ± 2 (↑26%)
4	Mg 2.5TiO_2 NPs	25 ± 2.5 (↓22%)	1.3 ± 0.3	64 ± 3 (↑28%)
5	Mg 2.5 TiO2 NFs	26 ± 3 (↓18%)	1.5 ± 0.4	72 ± 2 (↑44%)

* Percentage increase/decrease in the grain size and microhardness of Mg–TiO_2 nanocomposites containing TiO_2 reinforcements (NPs and NFs) are mentioned within brackets.

Table 4
Results of room temperature tensile testing.

Material	Reinforcement	0.2% TYS [MPa]	UTS [MPa]	Fracture strain [%]	Energy absorbed [MJ/m^3]
Pure Mg	Nil	89 ± 4.5	142 ± 6	10 ± 0.3	12 ± 1
Mg 1.98 TiO_2	NPs	88 ± 10	132 ± 8 (↓7%)	14.5 ± 1 (↑45%)	17.5 ± 0 (↑45%)
	NFs	80 ± 6 (↓10%)	130 ± 9 (↓8.5%)	13.5 ± 2 (↑35%)	16 ± 3 (↑33%)
Mg 2.5 TiO_2	NPs	91.1 ± 5 (↑3%)	134 ± 7 (↓5%)	6 ± 1 (↓40%)	8.6 ± 0.6 (↓29%)
	NFs	88 ± 5 (↓1%)	136 ± 2 (↓4%)	10 ± 1	12 ± 1

*Percentage increase/decrease in the tensile properties of pure Mg with addition of TiO_2 NPs and NFs are mentioned within brackets.

distributed TiO_2 reinforcements in the Mg matrix inducing grain boundary pinning thereby inhibiting recrystallized Mg grain growth. The fundamental principle behind the ability of fine inclusions in the metal matrix to nucleate recrystallized grains and to inhibit grain growth has been established already [35,36]. When compared to TiO_2 NFs, the presence of TiO_2 NPs within the Mg metal matrix is found to inhibit grain size of pure Mg more significantly with a maximum decrease of ~22% observed in the only marginally. The decrease in the CTE values observed in the Mg nanocomposites is due to: (a) reasonably uniformed distribution of TiO_2 reinforcements (Fig. 7) having lower CTE of ~9 × 10^{-6} K^{-1} [37] and (b) good interfacial integrity between the TiO_2 reinforcements and Mg metal matrix (Fig. 7). Further, when compared to TiO_2 NPs, presence of TiO_2 NFs within the Mg matrix appears to have considerable effect on lowering the CTE values of pure Mg and thereby improving its dimensional stability.

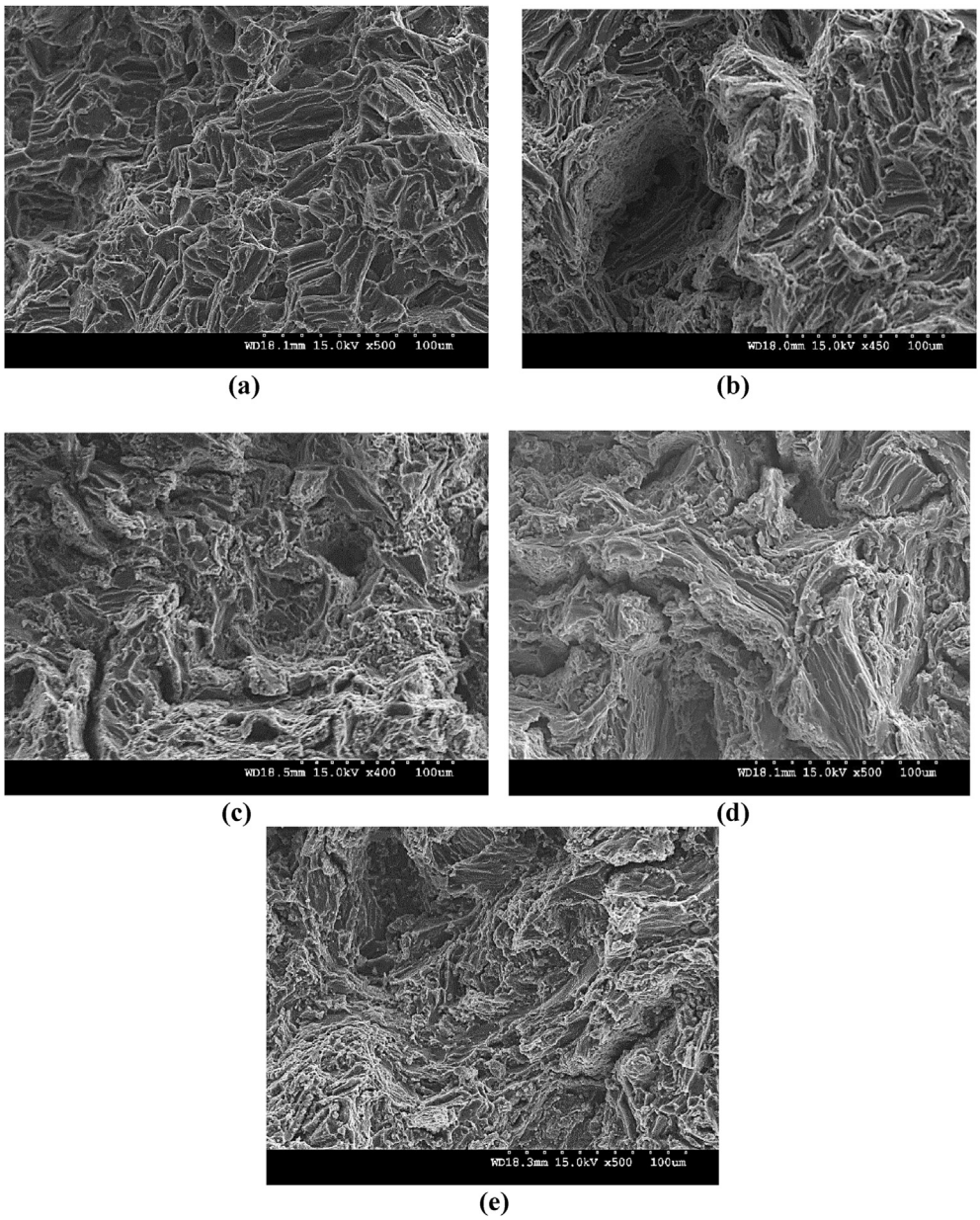

Fig. 9. Fractography images of pure Mg and Mg–TiO_2 nanocomposites after tensile loading: (a) Pure Mg, (b) Mg1.98TiO_2 NPs (c) Mg1.98TiO_2 NFs (d) Mg2.5TiO_2 NPs (e) Mg2.5TiO_2NFs.

Table 5
Results of room temperature compression testing.

Material	Reinforcement	0.2% CYS [MPa]	UCS [MPa]	Fracture strain [%]	Energy absorbed [MJ/m^3]
Pure Mg	Nil	76 ± 2	275 ± 4	20 ± 1.5	34 ± 4
Mg 1.98 TiO_2	NPs	89.9 ± 2 (↑18%)	245 ± 8 (↓10%)	25 ± 2 (↑25%)	46 ± 4 (↑35%)
	NFs	89.9 ± 7.4 (↑18%)	300 ± 9 (↑9%)	21 ± 0.5 (↑5%)	46 ± 6 (↑35%)
Mg 2.5 TiO_2	NPs	81 ± 0.6 (↑6)	233 ± 6 (↓15%)	24 ± 2 (↑20%)	37 ± 3 (↑9%)
	NFs	86 ± 1 (↑13)	294 ± 0.3 (↑7%)	24 ± 1 (↑20%)	52.2 (↑54%)

* Percentage increase/decrease in the compression properties of pure Mg with addition of TiO_2 NPs and NFs are mentioned within brackets.

3.5. Microhardness

The results of microhardness measurements of the synthesized Mg materials are shown in Table 3. Monolithic pure Mg exhibited the lowest microhardness value of 50 Hv and with the addition of TiO_2 reinforcements, the hardness value of pure Mg increased which is due to reasonably uniform distribution and high hardness (700 Hv) of TiO_2 reinforcements within the Mg matrix. Further, when compared to TiO_2 NPs, the presence of TiO_2 NFs significantly increases the hardness values of pure Mg by serving as a constraint

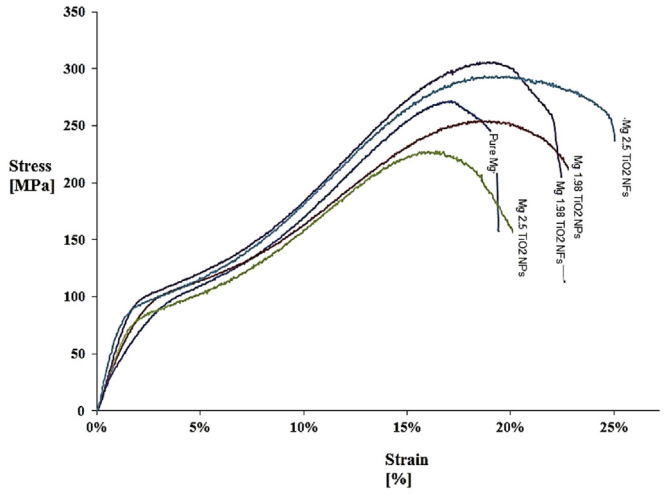

Fig. 10. Room temperature compression properties of Mg–TiO_2 nanocomposites containing TiO_2 NPs and NFs.

to localized deformation during indentation and as high as ~44% enhancement was observed in the case 2.5 vol. % TiO_2 NFs addition.

3.6. Tensile properties

Room temperature tensile properties of pure Mg and Mg (1.98 and 2.5) vol. % TiO_2 nanocomposites containing TiO_2 reinforcements in the form of NPs and NFs and their representative stress–strain curves are shown in Table 4 and Fig. 8, respectively. It is observed that the presence of TiO_2 reinforcements (NPs and NFs) marginally lowers the tensile strength of pure Mg. With addition of TiO_2 NPs, only a marginal increase in the tensile yield strength (0.2% TYS) of pure Mg was observed and Mg 2.5 vol. % TiO_2 nanocomposite exhibited the maximum 0.2% TYS of ~91 MPa. But, the ultimate tensile strength (UTS) of Mg–TiO_2 nanocomposites was found to be lower than that of pure Mg and similar observations were reported with Mg–TiO_2 nanocomposites containing TiO_2 NPs processed by disintegrated melt deposition technique (liquid synthesis) [38]. Whereas, the presence of TiO_2 reinforcements in the form of NFs affected both the 0.2% TYS and UTS of pure Mg (Table 4) with Mg 1.98 vol. % TiO_2 exhibiting ~80 MPa and ~130 MPa, respectively, which are lower than that of pure Mg by ~10 MPa.

The tensile fracture strain of pure Mg containing 1.98 vol. % TiO_2 NPs and NFs significantly increased by ~45% and ~35%, respectively. From the XRD studies (Table 2 and Fig. 5), the ratio of I/I_{max} corresponding to the basal plane intensity measured along the extrusion axis (longitudinal direction) of Mg 1.98 vol.% TiO_2 nanocomposite containing TiO_2 NPs and NFs is 0.655 and 0.878, respectively. This indicates that the presence of 1.98 vol. % TiO_2 reinforcements weakens the strong basal texture of pure Mg and thereby contributing to significant increase in the tensile fracture strain with limited or no improvement in the 0.2% TYS. Similar observations with Mg materials containing ultrafine reinforcements in the form of NPs have been reported previously [33,34,38]. With further addition of TiO_2 reinforcements (2.5 vol. %), the tensile fracture strain of pure Mg decreased and this may be due to: (a) dominance of strong basal texture of pure Mg observed through XRD studies with I/I_{max} corresponding to the basal plane intensity (Table 2) measured along the extrusion axis (longitudinal direction) of Mg 2.5 vol. % TiO_2 nanocomposite containing TiO_2 NPs and NFs of 0.844 and 1, respectively, (b) possible clustering of TiO_2 reinforcements within the Mg matrix and (c) increased nanocomposites porosity (Table 1). Mg 2.5 vol. % TiO_2 nanocomposite containing TiO_2 NFs exhibited higher tensile fracture strain when compared to that of Mg 2.5 vol. % TiO_2 with NPs which may be due to more reasonably uniform distribution of TiO_2 NFs (Fig. 7). Fig. 9 shows the fracture surfaces of pure Mg and Mg–TiO_2 nanocomposites under tensile loading. For all the synthesized Mg materials, the fractography image indicate cleavage mode of fracture highlighting that the fracture behavior of Mg composites is greatly controlled by the Mg matrix material. With the addition of TiO_2 reinforcements, refined fracture features when compared to that of pure Mg was observed.

The ability of a material to absorb energy up to fracture under tensile loading (EA) corresponding to the area under the stress–strain curve of pure Mg was found to increase with the addition of up to 1.98 vol. % TiO_2 reinforcements (NPs and NFs) which is due to: (a) marginal changes in the strengths of nanocomposite and (b) their higher tensile fracture strain. With further addition of TiO_2 reinforcements (2.5 vol. %), the energy absorbed (EA) was found to decrease and Mg 2.5 vol. % TiO_2 nanocomposite containing TiO_2 NPs exhibited EA of ~8.6 MJ/m3 which is ~29% lower than that of pure Mg. Among the synthesized Mg–TiO_2 nanocomposites, Mg 1.98 vol. % TiO_2 containing TiO_2 NPs exhibited the maximum of ~17.5 MJ/m^3 which is ~45% greater than that of pure Mg indicating their superior damage tolerant capabilities.

3.7. Compression properties

Room temperature compression properties of pure Mg and Mg (1.98 and 2.5) vol. % TiO_2 nanocomposites containing TiO_2 reinforcements in the form of NPs and NFs and their representative stress–strain curves are shown in Table 5 and Fig. 10, respectively. With the addition of TiO_2 reinforcements, increase in the 0.2% compressive yield strength (0.2% CYS) of pure Mg was observed with Mg 1.98 vol. % TiO_2 nanocomposite containing NPS and NFs exhibiting a maximum of ~90 MPa which is ~18% greater than that of pure Mg. But, the ultimate compressive strength (UCS) of Mg–TiO_2 nanocomposites containing TiO_2 NPs was found to be lower than that of pure Mg with Mg 2.5 vol. % TiO_2 nanocomposite exhibiting a minimum of ~233 MPa which is ~15% lower than that of pure Mg and similar observations with decrease in UCS of pure Mg was reported with Mg–TiO_2 nanocomposites processed by disintegrated melt deposition technique (liquid synthesis) [38]. Whereas, the presence of TiO_2 NFs was found to improve both the 0.2% CYS and UCS of pure Mg significantly with Mg 1.98 vol.% TiO_2 nanocomposite exhibiting a maximum 0.2% CYS and UCS of ~90 MPa and ~300 MPa, respectively which is ~18% and ~9% greater than that of pure Mg. The improvement in the UCS of pure Mg with addition of TiO_2 NFs may be due to the effective transferring of load from the Mg matrix to the TiO_2 NFs when compared to that of TiO_2 NPs [39]. For effective strengthening due to load bearing, when compared to that of NFs, higher volume fraction NPs in metal matrix nanocomposites is necessary [40]. Some of the important mechanisms that may be responsible for increase in the compression strength of Mg–TiO_2 nanocomposite are: (a) Orowan strengthening effect due to the presence of distributed TiO_2 NPs and NFs within the Mg matrix accounting for dislocation bowing [12,33,38,40], (b) Forest strengthening or mismatch in the CTE values between the Mg matrix and TiO_2 reinforcements leading to increase in the dislocation density [12,33,38,40], (c) Hall-Petch strengthening due to reduction in grain size (Table 3) [12,33,38,40] and (d) Taylor strengthening or mismatch in the modulus values between the Mg matrix and TiO_2 reinforcements [12,33,38,40].

The compressive fracture strain of pure Mg was found to increase with the addition of TiO_2 reinforcements with Mg 1.98 vol. % TiO_2 nanocomposite containing TiO_2 NPs exhibiting a maximum

compressive strain of ~25% which is ~25% greater than that of pure Mg. The ability of a material to absorb energy up to fracture under compressive loading (EA) corresponding to the area under the stress–strain curve (Fig. 9) of Mg–TiO_2 nanocomposites was found to be higher than that of pure Mg with Mg 2.5 vol. % TiO_2 nanocomposite containing NFs exhibiting a maximum of ~52 MJ/m^3 which is ~54% greater than that of pure Mg. Fig. 11 shows the fracture surfaces of pure Mg and Mg–TiO_2 nanocomposites under compressive loading. Fracture in pure Mg and Mg–TiO_2 nanocomposite was found to occur 45° with respect to the compression loading axis and their representative fractographs indicate presence of shear bands. No change in the fracture modes of Mg–TiO_2 nanocomposite samples containing TiO_2 NPs and NFs under compression loading was observed.

The tensile deformation of Mg materials is governed by slip mode with basal slip as the most dominant mechanism [33]. Whereas, under compression loading, due to the lower critically resolved shear stress (CRSS) to activate twinning, the initial deformation of Mg materials is by tensile twinning [33]. Thus, under room temperature loading, extruded Mg materials exhibit higher tensile yield strength but lower compressive yield strength and this is attributed to their strong basal texture (Fig. 5, Table 2) with basal planes parallel to the extrusion direction [41,42]. The tension-compression asymmetry (TCA) values of the synthesized Mg materials are shown in Table 6. The synthesized Mg–TiO_2 nanocomposites exhibited lower TCA values when compared to that of pure Mg (1.20) with Mg 1.98 vol. % TiO_2 nanocomposite exhibiting as low as 1.06 and 0.89 for TiO_2 NPs and NFs, respectively and thereby exhibiting weakening of basal texture of pure Mg. This allows non-basal cross slip activation to occur and thereby, among the synthesized Mg–TiO_2 nanocomposites, Mg 1.98 vol. % TiO_2 exhibited higher tensile fracture strain of ~14.5% and ~13.5% for TiO_2 in the form of NPs and NFs, respectively. With 2.5 vol. % addition of TiO_2 reinforcements (NPs and NFs), the TCA value of the

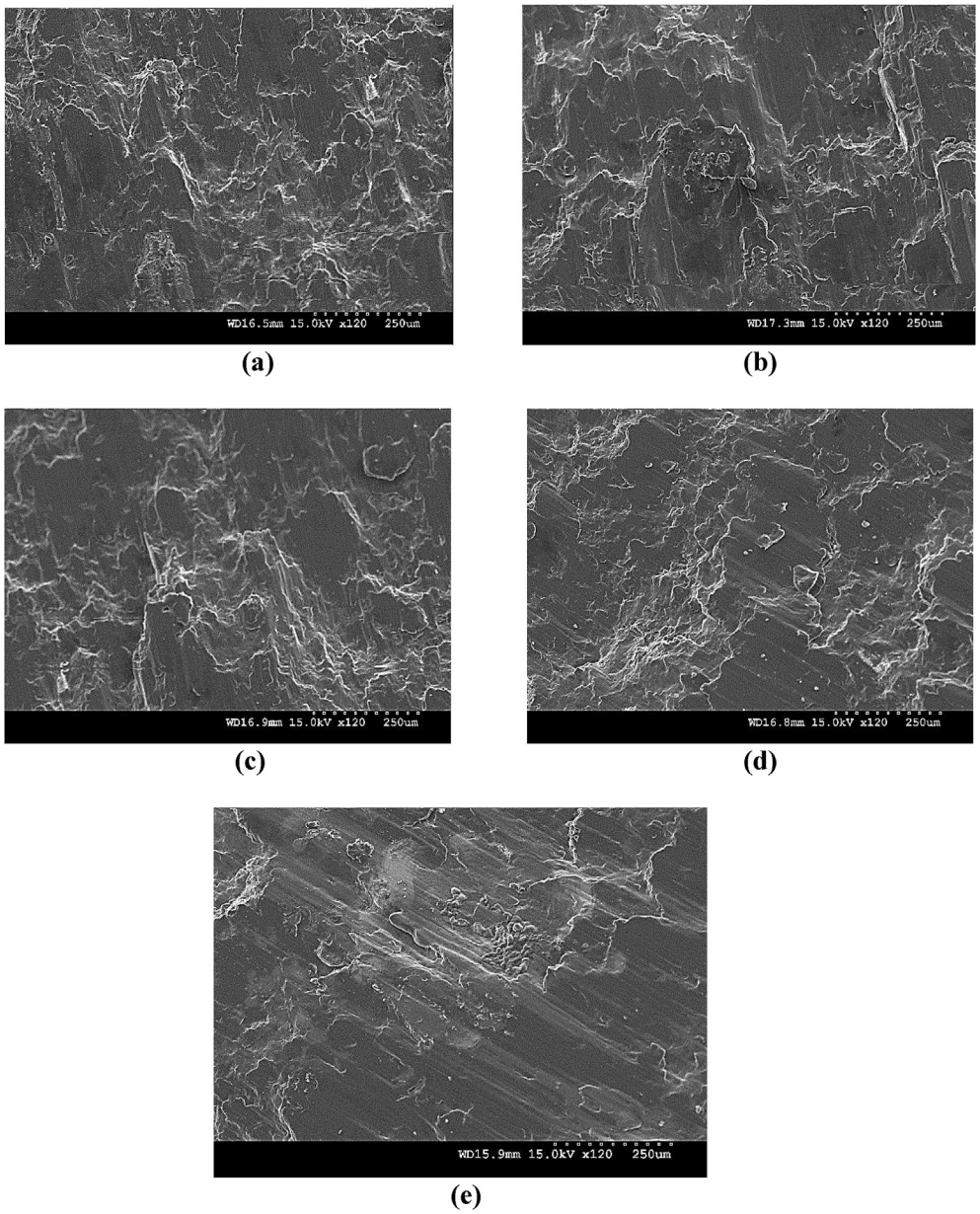

Fig. 11. Fractography images of pure Mg and Mg–TiO_2 nanocomposites after compression loading: (a) Pure Mg, (b) Mg1.98TiO_2 NPs (c) Mg1.98TiO_2 NFs (d) Mg2.5TiO_2 NPs (e) Mg2.5TiO_2NFs.

Table 6
Room temperature Tensile – Compression Asymmetry (TCA) of the synthesized pure Mg and Mg–TiO_2 nanocomposites.

Material	Reinforcement	$\sigma_{y,t}$ (MPa)	$\sigma_{y,c}$ (MPa)	TCA
Pure Mg	Nil	89 ± 4.5	76 ± 2	1.20
Mg 1.98 TiO_2	NPs	88 ± 10	89.9 ± 2	1.06
	NFs	80 ± 6	89.9 ± 7.4	0.89
Mg 2.5 TiO_2	NPs	91.1 ± 5	81 ± 0.6	1.13
	NFs	88 ± 5	86 ± 1	1.02

nanocomposites increased to 1.13 and 1.02, respectively, indicating the dominance of basal texture of pure Mg and thereby leading to a slight increase in its 0.2% TYS with significant decrease in its tensile fracture strain when compared to that of Mg 1.98 vol. % TiO_2.

4. Conclusions

In the present study, near dense Mg (1.98 and 2.5) vol. % TiO_2 nanocomposites containing TiO_2 reinforcements in the form of NPs and NFs are successfully synthesized utilizing powder metallurgy technique coupled with microwave sintering followed by hot extrusion and the effects of morphology of TiO_2 reinforcements on the physical, microstructural and mechanical properties of the Mg nanocomposite are studied. The primary conclusions of the current experimental findings as follows:

a) Through XRD studies, it is observed that morphology of ultrafine reinforcements play a vital role in texture modification of HCP metals such as Mg. Presence of 1.98 vol. % TiO_2 in the form of nanoparticulates contributed more to the weakening of strong basal texture of pure Mg with I/I_{max} value corresponding to the basal plane intensity measured along the extrusion axis (longitudinal direction) of the nanocomposite of ~0.655 when compared to that of Mg 1.98 vol. % TiO_2 nanocomposite containing TiO_2 nanofibers (0.878).
b) Significant grain refinement of pure Mg with the addition of TiO_2 reinforcements (NPs and NFs) was observed. TiO_2 in the form of nanoparticulates was found to decrease grain size of pure Mg more significantly with Mg 2.5 vol. % TiO_2 nanocomposite exhibiting a maximum decrease of ~25 μm which is ~22% lower than that of pure Mg.
c) Presence of TiO_2 in the form of nanofibers contributed significantly to the hardness values of pure Mg with Mg 2.5 vol. % TiO_2 nanocomposite exhibiting a maximum hardness value of ~72 Hv which is ~44% greater than that of pure Mg.
d) Under room temperature tensile loading, significant increase in the tensile fracture stain of pure Mg with addition of 1.98 vol. % TiO_2 reinforcements was observed with Mg 1.98 vol. % TiO_2 nanocomposite containing TiO_2 in the form of nanoparticulates exhibiting a maximum tensile fracture strain of ~14.5% which is 45% greater than that of pure Mg. Further addition of TiO_2 (2.5 vol. %) reinforcements significantly affected the tensile fracture strain of pure Mg. The presence of TiO_2 reinforcements within Mg matrix marginally affected its tensile strength properties by ~10 MPa with Mg 2.5 vol. % TiO_2 nanocomposite containing TiO_2 nanoparticulates exhibiting the maximum 0.2% TYS of ~91 MPa.
e) Under room temperature compression loading, the 0.2% CYS and compressive fracture strain of nanocomposites was found to be higher than that of pure Mg with Mg 1.98 vol. % TiO_2 nanocomposites containing TiO_2 in the form of both NPs and NFs exhibiting a maximum 0.2% CYS of ~90 MPa and fracture strain of ~25% (for 1.98 vol. % TiO_2 NPs), respectively. The UCS of Mg–TiO_2 nanocomposite containing TiO_2 in the form of NFs was found to be higher than that of pure Mg and nanocomposites containing TiO_2 NPs with Mg 1.98 vol. % TiO_2 nanocomposite (with NFs) exhibiting a maximum UCS of ~300 MPa which is ~9% greater than that of pure Mg.

Acknowledgments

One of the authors, Ganesh Kumar Meenashisundaram, sincerely thank National University of Singapore for the NUS Research Scholarship support towards his graduate studies. The authors also gratefully acknowledge Mr. Hardik Patel and Mr. Bhavesh Jain Lalwani from National Institute of Technology, Karnataka, Suratkal for their support and assistance towards sample preparation and successful completion of the project.

References

[1] M. Gupta, G.K. Meenashisundaram, Insight into Designing Biocompatible Magnesium Alloys and Composites: Processing, Mechanical and Corrosion Characteristics, Springer, 2015.
[2] R. Gehrmann, M.M. Frommert, G. Gottstein, Texture effects on plastic deformation of magnesium, Mater. Sci. Eng. A 395 (2005) 338–349.
[3] Z. Zachariah, S.S.V. Tatiparti, S. Mishra, N. Ramakrishnan, U. Ramamurty, Tension–compression asymmetry in an extruded Mg alloy AM30: temperature and strain rate effects, Mater. Sci. Eng. A 572 (2013) 8–18.
[4] H. Watanabe, K. Ishikawa, Effect of texture on high temperature deformation behavior at high strain rates in a Mg–3Al–1Zn alloy, Mater. Sci. Eng. A 523 (2009) 304–311.
[5] I. Ulacia, N. Dudamell, F. Gálvez, S. Yi, M. Pérez-Prado, I. Hurtado, Mechanical behavior and microstructural evolution of a Mg AZ31 sheet at dynamic strain rates, Acta Mater. 58 (2010) 2988–2998.
[6] J. Ferguson, F. Sheykh-Jaberi, C.-S. Kim, P.K. Rohatgi, K. Cho, On the strength and strain to failure in particle-reinforced magnesium metal-matrix nanocomposites (Mg MMNCs), Mater. Sci. Eng. A 558 (2012) 193–204.
[7] J. Umeda, M. Kawakami, K. Kondoh, E.-S. Ayman, H. Imai, Microstructural and mechanical properties of titanium particulate reinforced magnesium composite materials, Mater. Chem. Phys. 123 (2010) 649–657.
[8] S. Hassan, M. Gupta, Effect of particulate size of Al 2 O 3 reinforcement on microstructure and mechanical behavior of solidification processed elemental Mg, J. Alloys Compd. 419 (2006) 84–90.
[9] K. Deng, K. Wu, Y. Wu, K. Nie, M. Zheng, Effect of submicron size SiC particulates on microstructure and mechanical properties of AZ91 magnesium matrix composites, J. Alloys Compd. 504 (2010) 542–547.
[10] K. Deng, X. Wang, Y. Wu, X. Hu, K. Wu, W. Gan, Effect of particle size on microstructure and mechanical properties of SiCp/AZ91 magnesium matrix composite, Mater. Sci. Eng. A 543 (2012) 158–163.
[11] A. Sanaty-Zadeh, Comparison between current models for the strength of particulate-reinforced metal matrix nanocomposites with emphasis on consideration of Hall–Petch effect, Mater. Sci. Eng. A 531 (2012) 112–118.
[12] G.K. Meenashisundaram, M. Gupta, Low volume fraction nano-titanium particulates for improving the mechanical response of pure magnesium, J. Alloys Compd. 593 (2014) 176–183.
[13] S. Hassan, M. Gupta, Development of ductile magnesium composite materials using titanium as reinforcement, J. Alloys Compd. 345 (2002) 246–251.
[14] R. Rošic, P. Kocbek, J. Pelipenko, J. Kristl, S. Baumgartner, Nanofibers and their biomedical use, Acta Pharm. 63 (2013) 295–304.
[15] J. Fang, X. Wang, T. Lin, Functional Applications of Electrospun Nanofibers, InTech–Open Access Publisher, 2011.
[16] M. Ikegame, K. Tajima, T. Aida, template synthesis of polypyrrole nanofibers insulated within one-dimensional silicate channels: hexagonal versus lamellar for recombination of polarons into bipolarons, Angew. Chem. Int. Ed. 42 (2003) 2154–2157.
[17] Y. Hong, R.L. Legge, S. Zhang, P. Chen, Effect of amino acid sequence and pH on nanofiber formation of self-assembling peptides EAK16-II and EAK16-IV, Biomacromolecules 4 (2003) 1433–1442.
[18] P.X. Ma, R. Zhang, Synthetic Nano-scale Fibrous Extracellular Matrix, 1999.
[19] C.J. Ellison, A. Phatak, D.W. Giles, C.W. Macosko, F.S. Bates, Melt blown nanofibers: fiber diameter distributions and onset of fiber breakup, Polymer 48 (2007) 3306–3316.
[20] J. Fang, H. Wang, H. Niu, T. Lin, X. Wang, Evolution of fiber morphology during electrospinning, J. Appl. Polym. Sci. 118 (2010) 2553–2561.
[21] J. Fang, H. Niu, T. Lin, X. Wang, Applications of electrospun nanofibers, Chin. Sci. Bull. 53 (2008) 2265–2286.
[22] T. Lin, H. Wang, H. Wang, X. Wang, The charge effect of cationic surfactants on the elimination of fibre beads in the electrospinning of polystyrene, Nanotechnology 15 (2004) 1375.
[23] I.S. Chronakis, Novel nanocomposites and nanoceramics based on polymer nanofibers using electrospinning process—a review, J. Mater. Process.

Technol. 167 (2005) 283–293.
[24] G.E. Dieter, D. Bacon, Mechanical Metallurgy, McGraw-Hill, New York, 1986.
[25] A. Ravaglioli, A. Krajewski, Bioceramics, Springer, 1992.
[26] H. Kaneko, M. Uchida, H.M. Kim, T. Kokubo, T. Nakamura, Process of apatite formation induced by anatase on titanium metal in simulated body fluid, Key Eng. Mater. 218 (2001) 649–652.
[27] H.M. Kim, F. Miyaji, T. Kokubo, T. Nakamura, Preparation of bioactive Ti and its alloys via simple chemical surface treatment, J. Biomed. Mater. Res. 32 (1996) 409–417.
[28] M. McAlarney, M. Oshiro, L. Huang, Effects of titanium oxide properties on biocompatibility. A preliminary study, N. Y. State Dent. J. 59 (1993) 45.
[29] E.P. Ivanova, K. Bazaka, R.J. Crawford, New Functional Biomaterials for Medicine and Healthcare, Woodhead Publishing, 2014.
[30] C. Tekmen, I. Ozdemir, U. Cocen, K. Onel, The mechanical response of Al–Si–Mg/SiC p composite: influence of porosity, Mater. Sci. Eng. A 360 (2003) 365–371.
[31] S. Stock, B. Cullity, Elements of X-ray Diffraction, Prentice Hall, Upper Saddle River, New Jersey, 2001.
[32] K. Tun, P. Jayaramanavar, Q. Nguyen, J. Chan, R. Kwok, M. Gupta, Investigation into tensile and compressive responses of Mg-ZnO composites, Mater. Sci. Technol. 28 (2012) 582–588.
[33] G.K. Meenashisundaram, S. Sankaranarayanan, M. Gupta, Enhancing overall tensile and compressive response of pure Mg using nano-TiB2 particulates, Mater. Charact. 94 (2014) 178–188.
[34] G.K. Meenashisundaram, M. Gupta, Synthesis and characterization of High performance low volume fraction TiC reinforced Mg nanocomposites targeting biocompatible/structural applications, Mater. Sci. Eng. A (2015).
[35] P. Shewmon, Transformations, Metals, Indo American Books, 2006.
[36] R.E. Reed-Hill, R. Abbaschian, Physical Metallurgy Principles, 1973.
[37] J. González-Benito, E. Castillo, J. Caldito, Coefficient of thermal expansion of TiO< sub> 2 filled EVA based nanocomposites. A new insight about the influence of filler particle size in composites, Eur. Polym. J. 49 (2013) 1747–1752.
[38] G.K. Meenashisundaram, M.H. Nai, A. Almajid, M. Gupta, Development of high performance Mg-TiO< sub> 2 nanocomposites targeting for biomedical/structural applications, Mater. Des. (2014).
[39] G.E. Dieter, D. Bacon, Mechanical Metallurgy, McGraw-Hill, New York, 1986.
[40] G.K. Meenashisundaram, M. Gupta, Synthesis and characterization of high performance low volume fraction TiC reinforced Mg nanocomposites targeting biocompatible/structural applications, Mater. Sci. Eng. A 627 (2015) 306–315.
[41] G. Garcés, P. Pérez, P. Adeva, Effect of the extrusion texture on the mechanical behaviour of Mg–SiC p composites, Scr. Mater. 52 (2005) 615–619.
[42] G. Garcés, M. Rodríguez, P. Perez, P. Adeva, Effect of volume fraction and particle size on the microstructure and plastic deformation of Mg–Y 2 O 3 composites, Mater. Sci. Eng. A 419 (2006) 357–364.